Oral Radiology (2022) 38:17–28
https://doi.org/10.1007/s11282-021-00521-x

REVIEW ARTICLE

Actual applications of magnetic resonance imaging in dentomaxillofacial region

Migi Johnson[1] · **L. S. Sreela**[1] · **Philips Mathew**[1] · **Twinkle S. Prasad**[1]

Received: 22 November 2020 / Accepted: 13 February 2021 / Published online: 26 February 2021

Abstract

Magnetic resonance imaging (MRI) is a versatile imaging modality utilized in various medical fields. Specifically used for evaluation of soft tissues, with non-ionizing radiation and multiplanar sections that has provided great guidance to diagnosis. Nowadays, use of MRI in dental practice is becoming more pervasive, especially for the evaluation of head-and-neck cancer, detection of salivary gland lesions, lymphadenopathy, and temporomandibular joint disorders. Understanding the basic principles, its recent advances, and multiple applications in dentomaxillofacial region helps significantly in the diagnostic decision making. In this article, the principle of MRI and its recent advances are reviewed, with further discussion on the appearance of various maxillofacial pathosis.

Keywords Magnetic resonance imaging · Diffusion-weighted MRI · MR spectroscopy · Salivary gland neoplasms · Oral cancer

Introduction

Tremendous technological advances in medical imaging over the past several decades lead the way to the introduction of three-dimensional imaging in the field of dentistry. MRI is superior to other imaging modalities, due its ability to depict the soft tissues and functional changes without any ionizing radiation. MRI have experienced rapid development and found wide dental applications in recent years. Evolution of conventional MRI to newer advances techniques such as diffusion-weighted imaging (DWI), perfusion weighted imaging (PWI), MR spectroscopy (MRS), and functional MRI (fMRI) enabled dental researchers to narrow down the diagnostic possibilities. Adequate knowledge of dental applications overwhelms the limited use of MRI. The purpose of this article is to inform about the basic principle of conventional and advanced MRI along with specific clinical applications of MRI in different field of dentistry.

✉ Migi Johnson
migicj1990@gmail.com

[1] Department of Oral Medicine and Radiology, Government Dental College Kottayam, Gandhinagar, Kottayam 686008, Kerala, India

Materials and methods

An initial search was performed using the search terms MRI, DWI, PWI, MRS, fMRI, head-and-neck cancer, salivary gland pathology, temporomandibular joint disorders, cervical lymphadenopathy, nerve injury, vascular lesions, bony lesions, and pre-implant assessments in the PubMed, Medline, Scopus, and Google Scholar. 153 articles were analyzed and 63 articles were included.

Formation of MRI

Magnetic resonance imaging is based on the physics of nuclear magnetic resonance (NMR) which was first depicted by both Bloch and Purcell in 1946 [1]. The simplest atom, hydrogen consists of single proton in nucleus and single circulating electron orbiting around the proton. Individual protons in the nuclei of all atoms possess a spin, or angular momentum. Since the spin is associated with an electrical charge, a magnetic field is generated in nuclei known as magnetic dipole moment. In the atoms of biologic molecules, the protons in the nucleus are randomly arranged, canceling the dipole moment each other, and therefore usually do not exhibit any magnetic property. We have a lot of hydrogen atoms in our body, especially in the form of water, and energy storing molecules of fat and carbohydrates.

When an external magnetic field is applied, all the protons line up. Most of them align in the direction of the magnetic field, which is parallel to the external magnetic field—spin up, and others align anti-parallel (opposite) with the magnetic field, spin down. These orientations correspond to low-energy and high-energy states of the dipoles, respectively. These protons rotate like spinning top and the rate of precession depends on Larmor frequency equation which states that the rate of rotation is directly proportional to the applied magnetic field. The Larmor frequency of hydrogen is 42.58 MHz in a magnetic field of 1 T. Initially, half the protons will be with and against the magnetic field, where the system is not in equilibrium. To attain equilibrium, over the time, more protons align with magnetic field by attaining a lower energy state by releasing energy to lattice. This energy release is known as *T1* or spin lattice relaxation. Now, the magnetization of the patient in the direction of external magnetic field which is known as longitudinal magnetization representing the z-axis cannot be measured directly. When a radiofrequency (RF) pulse of same magnitude of the precession of proton is applied, some protons absorb energy and flip into high-energy state, and as a result, the longitudinal magnetization decreases to zero as the opposing magnetic forces cancel each other. Additionally, RF pushes the proton to synchronous and spin together to produce a net transverse magnetization in the x–y plane which can be measured by RF coil. After the RF pulse is switched off, protons being positively charged repel each other and move apart which loses transverse magnetization, this process is known as *T2* or spin–spin relaxation. The loss of signal intensity due to dephasing of the proton in the receiving coil is the free induction decay. Then, the protons go back from their high to low state of energy, so the longitudinal magnetization increases and grows back to its original value [2].

Pulse sequences

*T*1 and *T*2 (and partially *T*2 *) are intrinsic parameters of the tissues, and they have different values based on different tissues and may be altered by pathology, which provide image contrast. A wide variety of MRI pulse sequences is accomplished by administering RF pulses and magnetic field gradients that result in a set of images with different geometric characteristics and contrasts. T1-weighted images (T1WI) and T2-weighted images (T2WI) are the common sequences usually used for anatomic images and pathologic images, respectively. In T1WI, fatty tissue appears as hyperintense signal (bright), muscles, and soft tissue as intermediate signal (gray) and fluid as hypointense signal (black). T2WI produces increased signal from pathologic tissue, due to the increased water content. Fat-suppressed T1 and T2-weighted image are used to eliminate the hyperintense fat signal and for detection of other hyperintense tissue signals. Fat saturation, short T1 inversion recovery (STIR), water excitation, and subtraction are fat suppression methods. In contrast-enhanced T1-weighted image, a gadolinium-based contrast agent is injected intravenously, to shorten the T1 and T2, thereby increasing the tissue signals and bright images are obtained. Proton density images are not weighted to either T1 or T2 character, which represent an overall density of hydrogen, commonly used for TMJ imaging, because they offer an excellent signal distinction between fluid, hyaline cartilage, and fibrocartilage [3]. The signal that comes back from the patient is collected as echo. Echos are produced in two ways by the pulse sequence; spin echo (SE) and gradient echo (GE). Spin echo includes 90º pulse followed by one or more 180º refocusing pulses. Fast (or turbo) spin echo (FSE), a variation of SE used to speed up the process. GE varies from spin echo in regards to the flip angle usually below 90º and the absence of a 180º rephrasing pulse. Fast low-angle shot (FLASH) and fast imaging with steady-state precession (FISP) are variations of GE. Spin echo produces quality images, while gradient echo gives faster images.

Recent advances

Recent advances in the field of MRI include DWI, PWI, MRS, and fMRI which have a greater role in assessment of oral lesions.

Diffusion-weighted imaging depicts the random translational motion of water molecules in biological tissues performed with an EPI (echo planar imaging) sequence and a linear regression after a logarithmic transformation of the signal intensity was used to calculate the apparent diffusion coefficient (ADC) values. Variation in ADC values reflects the diffusion of water molecules between intracellular and extracellular compartments of a tissue. At least two *b* values (degree of diffusion weighting applied) are needed to analyze the motion of water, which represents the duration between the gradient pulses used. Most commonly, *b*0 and *b*800 or *b*1000 values are used for head-and-neck imaging. Acquiring multiple *b* values' techniques such as intravoxel incoherent motion (IVIM) and diffusion kurtosis imaging (DKI) are employed. IVIM imaging can distinguish between pure molecular diffusion and motion of water molecules in the capillary network. DKI represents the extent to which the diffusion pattern of the water molecules deviates from a perfect Gaussian curve that is assumed by calculating standard ADC values [4].

Perfusion is defined as the steady-state delivery of blood to tissue. Some of the perfusion techniques available are dynamic contrast-enhanced (DCE) perfusion, dynamic susceptibility contrast (DSC) perfusion, and arterial spin labeling (ASL). DCE perfusion is most commonly used for the head-and-neck area exploiting the T1 relaxivity effects

of contrast agents which is able to characterize perfusion and vascularization of tissues. DSC perfusion exploits the susceptibility-induced signal loss after the administration of contrast on T2-weighted sequences. Magnetically labeled arterial blood water is used as a diffusible flow tracer in ASL, which could reflect neovascularity and angiogenic activity of lesion.

Magnetic resonance spectroscopy is a non-invasive method which allows us to analysis tissue metabolite concentration in tissues and organs. 1H and 31P are the main nuclei investigated in clinical MRS, but 13C, 23Na, and 19F are also amenable to MRS investigation. Proton MRS (1H-MRS) is the most commonly used method typically based on the detection of elevated levels of choline, lactate, N-acetyl-aspartate, myo-inositol, creatine, glutamine and glutamate. The concentrations of metabolites in MRS are expressed either as absolute values or ratios [5].

Application and efficacy of MRI in maxillofacial region

Magnetic resonance imaging can be utilized for the assessment of salivary gland pathology, head-and-neck cancer, temporomandibular joint disorders, cervical lymphadenopathy, swelling in the orofacial region, nerve injury, vascular lesions, bony lesions, and pre-implant assessments. Besides, dental MRI is a newer non-invasive diagnostic method for evaluating the pulpal and periapical changes.

Salivary gland pathology

Magnetic resonance imaging of salivary gland is superior to other imaging modality due to its excellent spatial resolution, superior soft-tissue contrast, and multiplanar evaluation of gland. MR images are preferred for differentiating benign from malignant lesions, intraglandular from extraglandular lesions, demarcation of tumor–muscle interface, and facial nerve with relation to the tumor. T1, T2, and postcontrast fat-suppressed imaging with T1 weighting is recommended for salivary gland imaging for delineation of lesions and prediction of the nature of gland pathology. The key MRI findings in various salivary gland pathologies are summarized in Table 1. Contrast administration helps to distinguish between solid and cystic lesions, and perineural extension of lesion, and to evaluate the margins of the mass and its extension into surrounding tissue planes [6]. Figure 1 shows fat-suppressed images with heterogeneous mass of adenoid cystic carcinoma. Newer imaging techniques that increase the efficacy of diagnosis are DWI, PWI, MRS, and MR sialography. DWI evaluates the diffusion occurs as a result of the constant movement of water molecules in the tissue provide useful information about gland pathology. Variation

Table 1 Key MRI findings in various salivary gland pathologies

Lesions	MR findings
Sialolithiasis	Stone appear as low signal on all sequences, outlined by high-signal saliva on T2 On MR sialography, appear as hypointense structure surrounded by hyperintense saliva
Sialadenitis	Acute; low signal on T1 and high signal on T2 Chronic; heterogeneous low signal on T1 and low-to-intermediate on T2
Sjögren's syndrome	Early stage; enlarged homogenous glands Intermediate stage; enlarged inhomogeneous multiple hypointense mixed with hyperintense signal (salt and pepper appearance) on T2 Advanced stages; inhomogeneous with overall decreases on T2 signals (honeycomb pattern)
Pleomorphic adenoma	Homogeneous, intermediate-to-low T1 signal, hyperintense if hemorrhagic Heterogeneous high T2 signal, whereas peripheral capsule show low T2 signal Mild to moderate contrast enhancement Dynamic contrast curve shows quick uptake, then plateau(contrast retention)
Warthin's tumors	Low signal in both solid and cystic components on T1, Cystic areas may show high signal due to debris or hemorrhage Intermediate to high T2 signal in solid component and high T2 signal in cystic foci Minimal contrast enhancement of solid components In DWI, ADC values are lower than benign mixed tumor but similar to carcinoma In DCE, rapid enhancement with rapid washout
Mucoepidermoid carcinoma	On T1, low-grade shows heterogeneous, well-defined mass with predominantly low signal and high-grade as solid, infiltrative mass with intermediate signal Low-grade form depict heterogeneous low T2 signal with cystic areas as high T2 signal and high grade as intermediate signal with infiltrating mass Heterogeneous contrast enhancement In DWI, ADC values are lower than benign mixed tumor but similar to Warthin tumor
Adenoid cystic carcinoma	Low to intermediate T1 signal intensity and moderate T2 signal intensity Homogeneously enhancing mass

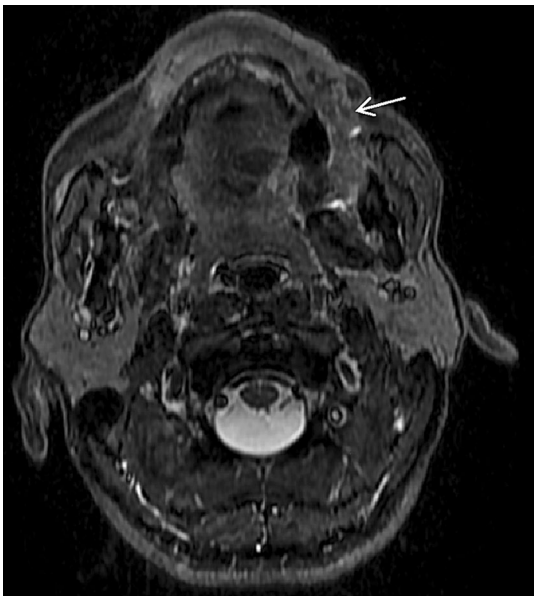

Fig. 1 Axial STIR fat-suppressed images demonstrates heterogeneous mass involving upper buccal mucosa and buccal space suggestive of adenoid cystic carcinoma of left buccal mucosa

of ADC values in diseases like sialadenitis, Sjögren's syndrome, and benign and malignant gland tumors helps to differentiate one lesion from another. Perfusion is a marker of physiologic or pathologic processes, assessed in salivary gland pathology by analyzing the time-signal intensity curve (TIC) after DCE MR imaging. Yabuuchi et al. evaluated all different parotid tumors and described four TIC patterns; Type A (persistent) time to maximal enhancement was more than 120 s after contrast administration, seen in pleomorphic adenoma; type B (washout) time to peak was 120 s or less with high washout ratio (—> 30%), characteristic of Warthin tumors as well as carcinomas; type C (plateau) time to peak was 120 s or less with low washout ratio (< 30%), found in malignant lesions; type D: (flat) are usually benign [7]. Yabuuchi et al. showed that the sum of the TIC patterns and ADC values significantly increases the differentiation between benign and malignant parotid tumors. Pleomorphic adenoma show ADC value > 1.4 and type A perfusion curve whereas Warthin tumor will have ADC value < 1 and type B perfusion curve. Type C perfusion curve represent low-grade and high-grade malignant tumor in which low grade shows high ADC value (1–1.4) and high grade with low ADC value (< 1) [8]. Various studies assessing salivary gland pathologies with newer MRI techniques is mentioned in Table 2 [7, 9–17].

Oral cancer

Main imaging features to be assessed in MRI for oral cancer are epicenter and tumor thickness, involvement to surrounding tissues such as muscle, neurovascular bundle, bone, and extension across the midline. MR images of osseous involvement include loss of low-signal-intensity

Table 2 Studies assessing salivary gland lesions by use of newer MRI techniques

Imaging	Uses	Author
DWI	Benign neoplasms presents higher ADC values compared with malignant and Warthin tumors The differentiation between benign versus malignant neoplasms, using a cut-off ADC value of 1.50×10^{-3} mm^2/s presented 74.1% accuracy	Khamis et al. [9]
	DWI with gustatory stimulation could noninvasively evaluate the functional changes of salivary glands following RT	Zhang, Y et al. [10]
	DWI is a promising tool to allow differentiation between the early and advanced disease. Higher ADCs were determined for early stage Sjögren's syndrome (SS) and advanced disease revealed significantly lower ADCs	Reiger et al. [11]
	DWI allows differentiation between reactive inflammatory and neoplastic lesions of the parotid glands	Terra et al. [12]
	IVIM parameters depict malignant tumors had significantly smaller value than pleomorphic adenomas, and for Warthin tumors ,it was even smaller	MisaSumi et al. [13]
Perfusion MR	TIC from DCE helps in differentiating malignant from benign salivary gland tumors in which malignant tumors show early enhancement and low washout, benign pleomorphic adenomas demonstrated gradual enhancement, and Warthin tumors exhibited early enhancement and high washout	Yabuuchi et al. [7]
	DCE has the potential to quantify microvascular function in SS and to differentiate the SS and non-SS patients	Roberts et al. [14]
MRS	Choline/creatine (Cho/Cr) ratios greater than 2.4 at an echo time of 136 ms, a distinction between benign and malignant lesions is possible, while a ratio greater than 4.5 suggests Warthin tumor	King et al. [15]
MR sialography	MR sialography can replace conventional sialography for diagnosing and staging SS and give information on different aspects of glandular and duct pathology	Ahmed et al. [16]
	MR sialography is useful for diagnosing sialolithiasis and sialadenitis with less failure rate compared to digital subtraction sialography although it has superior diagnostic information	Kalinowski et al. [17]

cortex, replacement of high-signal-intensity marrow on T1 intermediate-signal-intensity tumor, contrast enhancement within bone, and contrast enhancement of nerves traversing the mandible, especially the inferior alveolar nerve. In perineural spread, the involved nerve may appear enlarged on contrast-enhanced images [18]. Figure 2 demonstrates contrast-enhanced T1 MRI image of squamous cell carcinoma of tongue with hyperintense signal. Variation in ADC values in DWI helps in characterization of tumors, to differentiate viable and necrotic parts of malignant tumors, to distinguish between recurrent or residual tumors from post-treatment changes, in prediction and monitoring early treatment response [19]. In PWI, DCE parameter K_{trans} (volume transfer constant), ve (fractional volume of extravascular-extracellular space per unit volume of tissue), and vp (fractional volume of the plasma space) values are useful for differentiating malignant lesions and to predict treatment response [20]. Choline being a marker of proliferation and cell membrane turnover, elevated levels of choline metabolite provide good diagnostic value for 1H-MRS in cancer [21]. Role of newer MRI technique in assessing the oral cancer was briefly described in Table 3 [22–32].

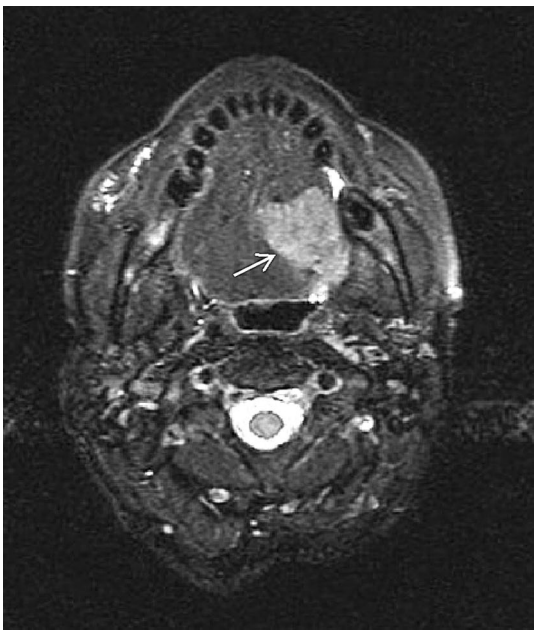

Fig. 2 Axial contrast-enhanced T1 MRI image demonstrates squamous cell carcinoma in left posterior aspect of tongue extending to midline

Lymph nodes

Normal unchallenged nodes are only a few millimeters in size and may not be seen on imaging. Normal lymph nodes depicted in MRI are markedly hypointense to surrounding fat on T1, moderately hypointense on PD images, and isointense or moderately hyperintense on T2. Iron-oxide particles, when injected intravenously, can gain access to lymph nodes, and the metastatic lymph nodes appear hypointense, while normal lymph nodes clear the iron oxide particles. Figure 3 demonstrates contrast-enhanced T1 MRI image a left nasopharyngeal carcinoma with level 1 lymph node with hyperintense signal on periphery and hypointense signal toward center. Studies have reported the ability of DWI to discriminate malignant from benign lymph nodes, with the metastatic nodes exhibiting lower ADC values. In MRS, average Cho/Cr ratio in

Table 3 Role of MRI in oral cancer management

Imaging	Uses	Author
DWI	Mean ADC value of benign solid lesions was significantly higher than that of malignant tumors with threshold ADC value of 1.22×10^{-3} mm^2/s	Wang et al. [22]
	Mean ADCvalue of recurrent/residual tumors was less than that of posttherapeutic changes with threshold value of 1.30×10^{-3} mm^2/s	Razek et al. [23]
	ADC values can accurately differentiate persistent or recurrent tumors from nontumoral tissue, both in the early (<4 months) as well as the late (>4 months) postradiation therapy period	Vandecaveye et al. [24]
	Pretreatment mean ADC value of complete responders ($1.04\pm0.19\times10^{-3}$ mm^2/s) was significantly lower than that of patients who exhibited a partial or no response ($1.35\pm0.30\times10^{-3}$ mm^2/s)	Kim et al. [25]
Perfusion MR	K_{trans} and ve value on DCE shows significant difference thereby distinguishing SCC from lymphoma	Mina park et al. [26]
	Skewness of K_{trans} on pretreatment DCE was the strongest predictor of treatment response for stage IV patients	Shukla-Dave et al. [27]
	ASL technique could accurately determine the effect of nonsurgical treatment	Fujima et al. [28]
MRS	Elevated Cho/Cr ratios have been demonstrated consistently in carcinoma compared with normal tissues	Mukherji et al. [29]
	Benign neoplasms have higher Cho/Cr than the malignant ones	Yu Q et al. [30]
	Poor tumor response showed elevated Cho/Cr ratios	Bezabeh et al. [31]
	Cho levels after chemo-radiotherapy may serve as a marker of residual cancer	King et al. [32]

Fig. 3 Axial contrast-enhanced T1 MRI image demonstrates a left nasopharyngeal carcinoma with level 1 lymph node

the metastatic lymph nodes was significantly higher than that for benign lymphoid hyperplasia, and also, lipid and lactate act as biomarkers for metastatic nodes [33]. The evaluation and characterization of cervical lymph nodes includes determination of nodal location, evaluation of nodal morphology, and its functional activity. The morphologic parameters such as shape, inhomogeneity, size, extranodular spread, clustering, and sentinel location are evaluated [34].

Temporomandibular joint disorders

Now, MRI has been confirmed as best imaging modality for TMJ assessment, as it allowed better visualization of localization of the disk, retrodiskal layer, and lateral pterygoid attachments. Both direct signs such as abnormal disk morphologic features, disk displacement, joint effusion, osteoarthritis as well as indirect signs like, thickening of an LPM attachment, and rupture of retrodiskal layers of TMJ dysfunction can be depicted. On T1, meniscus show homogeneous low-signal intensity, bilaminar zone as intermediate signal intensity, and anterior band and the intermediate zone as hypointense, and the posterior band is slightly hyperintense, while in disk diseases, posterior band will be hypointense. Proton density fat-supressed images are shown in Fig. 4a in closed mouth sequences demonstrate anteriorly displaced right articular disk and (b) in open mouth sequences shows no significant movement of articular disk suggestive of anterior displacement with no reduction. Joint effusion was best depicted on T2, manifesting as areas of hyperintensity [35]. The accuracy of MRI in evaluating osseous changes in TMJ was from 60% to 100%, and the accuracy in evaluating disk displacement was from 73% to 95% [36]. Standard protocol for MRI diagnosis of anterior disk displacement uses the most superior surface (12 o'clock position) of the condyle as a reference point for the posterior band of the disk. A posterior band of the disk located anterior to the 12 o'clock position correlates to anterior disk displacement [37]. Studies on

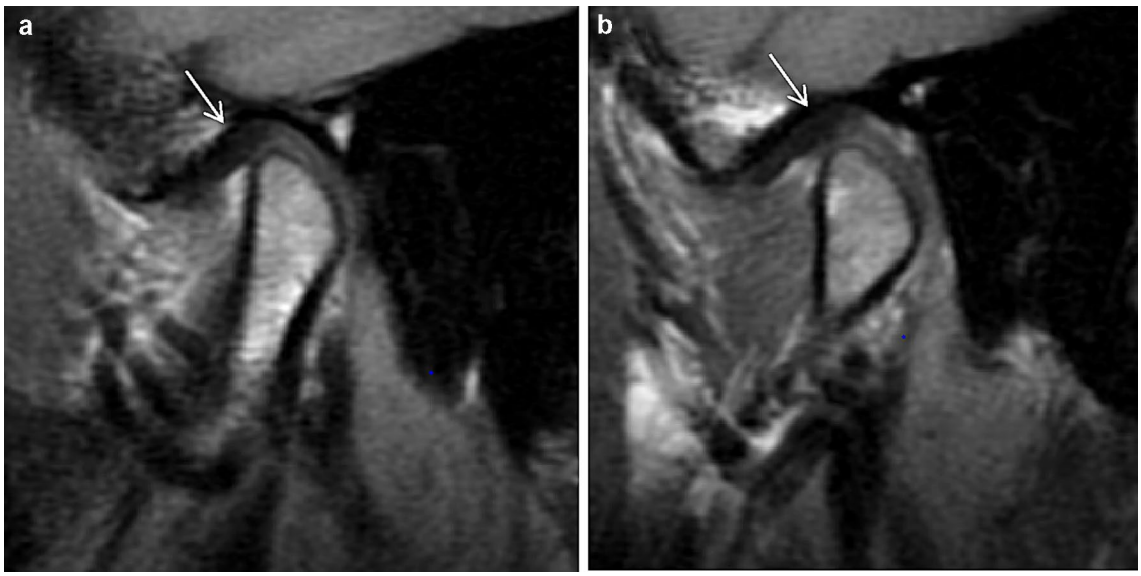

Fig. 4 Sagittal proton density fat-supressed images (**a**) in closed mouth sequences demonstrate anteriorly displaced right articular disk and **b** in open mouth sequences shows no significant movement of articular disk suggestive of anterior displacement with no reduction

MR arthrography with the intra-articular injection of gadopentate dimeglumine are superior in detecting adhesions and perforation of the TMJ [38]. Novel real-time MRI based on FLASH offers access to TMJ dynamics, both mandibular condyle movement and disk displacements [39].

Vascular lesions

Bhat V et al. suggested that hemangioma shows well-defined hypointense T1 signal, lobulated T2 hyperintense signal with central low-intensity dot sign with marked enhancement [40]. In AV malformation, T1 and T2 produce signal void, while dynamic contrast MR angiography demonstrates the feeding vessels. Ill-defined T1 hypointense and T2 hyperintense lesion with ill-defined tissue planes, muscle, and bone involvement is presented in venous malformations. Lymphatic malformations show T1 hypointense and T2 hyperintense multilocular lesions with ill-defined margins and variable enhancement of septae. Dong MJ et al. analyzed significant difference between ADC values of hemangioma and venous malformation in which venous malformation shows higher value [41].

Neural lesions

Peripheral nerve evaluation and characterization of neuropathies can be assessed by MR neurography which involves high-field-strength imaging (ideally 3 T) with the use of both two-dimensional and three-dimensional (3D) imaging including nerve-selective imaging and diffusion imaging. In peripheral nerve evaluation, based on the degree of nerve injury, T2 signal varies from homogenous to heterogeneous hyperintensity along with associated muscle denervation as reported by Chhabra et al. [42]. Schwannomas appear heterogeneously hyperintense on T2 due to the variable cellular and water content of type A and B Antoni cells and hypointensity on T1 [43].

Soft-tissue masses

Ranula shows well-defined homogenous low or intermediate signal on T1 and high signal on T2, as shown in Fig. 5 [44]. Lipoma presented with high signal, isointense with subcutaneous fat, on both T1 and T2. Well-defined, heterogeneous low signal on T1 and markedly high signal on T2 are seen on dermoid cyst while the cervical cyst as well defined, homogeneous intermediate signal on both T1 and T2.

Bony lesions

Boeddinghaus R et al. reported that in acute osteomyelitis, MRI shows high sensitivity in detecting cancellous marrow abnormality, results in reduced T1 signal, increased

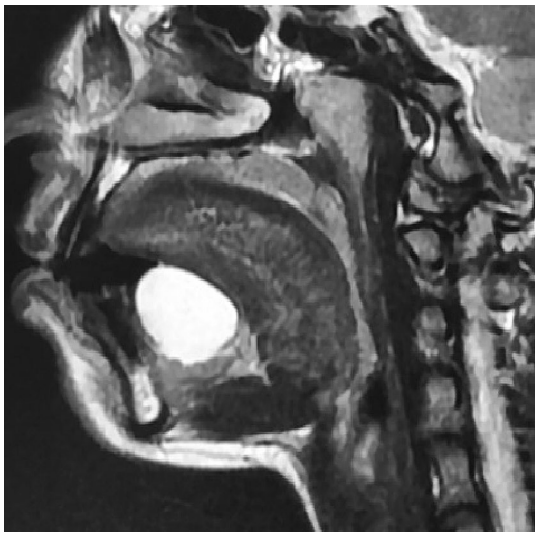

Fig. 5 Sagittal T2 images demonstrate hyperintense signal with moderate enhancement in right sublingual space above mylohyoid muscle suggestive of minor salivary gland retention cyst (Ranula)

T2 signal, and contrast enhancement of bone and the adjacent inflamed soft tissues. Post-gadolinium-enhanced T1-weighted MRI of chronic osteomyelitis distinguishes sequestra from normal cortical bone and demonstrates periosteal inflammation, important in planning decortication surgery [45]. In osteonecrosis, signal shows low-intensity areas in T1 and high-intensity signal in STIR sequences [46]. Osteoradionecrosis provide homogeneous low marrow signal due to fibrosis on T1. T2 shows heterogeneous signal with increased T2 for marrow oedema and reduced T2 for marrow sclerosis and fragmentation of bone and sequestration with very low signal on all sequences, as well as contrast enhancement after injection of gadolinium. ORN can be differentiated from tumor recurrence with DWI (high ADC values in necrosis as opposed to low ADC values in tumors).

Follicular cysts include variable signal intensity on T1 due to variable protein content within the cyst, high signal on T2, and occasionally slight enhancement of the thin cyst wall. In KCOT due to the variable protein content, intermediate signal intensity may be seen on T1, heterogeneous signal on T2, and mild contrast enhancing rim that facilitate differentiation from ameloblastoma. In DWI, high ADC value noted for benign cystic masses compared to solid masses may be due to the free mobility of water proton in the fluid. Langerhans cell histiocytosis show hypointense signal on T1, hyperintense signal on T2 and marked contrast enhancement. ADC values are usually slightly higher than in malignant lesions ($\geq 1.2 \times 10^{-3}$ mm^2/s versus $\pm 1 \times 10^{-3}$ mm^2/s). CGCG has a homogeneous or slightly heterogeneous intermediate signal on T1, T2, and STIR, and shows moderate-to-strong contrast enhancement. Primary intraosseous SCC

shows solid tumor portions with lower signal on T2, whereas cystic portions display a high signal. Contrast enhancement of solid portions is typically seen, as well as infiltration into the perimandibular soft tissues. ADC values of solid parts are low, suggesting tumor components with high cellularity [47]. The key MRI findings in various bony lesions are summarized in Table 4.

Inflammation

Space infections were assessed by comparing shape and signal intensities of the fascial spaces of the unaffected sides. An abscess show one or more areas of low T1 signal or high T2 signal with peripheral enhancement [48]. Cellulitis demonstrates diffuse linear or ill-defined soft-tissue thickening with hyperintensity on both T2 and STIR and hypointensity on T1 and contrast enhancement [49].

Muscle disorder

Muscle commonly appears as low-signal intensity on both T1- and T2-weighted images with fat suppression except lingual muscles, which has intermediate signal intensity on T1-weighted images due to their relatively high-fat component compared to other muscles. Zhang S et al. proposed that newer real-time MRI help to assess the normal swallowing patterns and abnormal orofacial muscle function [50]. Ekprachayakoon et al. suggested that dynamic MRI is useful in dentistry to evaluate the relationship between tongue function and maxillofacial morphology for orthodontic treatment and orofacial myofunctional therapy, and also for improving tongue movement during speech therapy [51]. Sawada et al. suggest that DWI could be used to assess myalgia of the masticatory muscles quantitatively. The ADC values of the masticatory muscles on the pain side were significantly greater than those of the contralateral side without pain [52]. Masticatory muscles usually demonstrate increased T2 signal and post-gadolinium enhancement after

Table 4 Key imaging findings in bony lesions

Lesion	T1WI	T2WI	T1WI C +
Osteoradionecrosis	Homogeneous low signal in marrow	Variable high signal in marrow	Irregular enhancement
Osteonecrosis	Low signal intensity	Variable signal depending on stage. Often high-signal intensity	Enhancement in bone and surrounding soft tissues
Follicular cyst	Low-to-intermediate signal intensity	Hyperintense signal	Slight enhancement of the thin cyst wall
Odontogenic keratocyst	Intermediate signal intensity	Heterogeneous, low-to-high-signal intensity	Thin enhancing rim
Buccal bifurcation cyst	Low to intermediate signal intensity	Increased signal intensity	
Aneurysmal bone cyst	Subacute blood; hyperintensity	Fluid–fluid levels	Solid periphery with intense enhancement
Ossifying fibroma	Intermediate to low signal Fibrous areas; intermediate signal. Radiopaque areas; hypointense	Mixed low and high signal Fibrous areas hyperintense (usually lesion center). Osseous/cemental areas hypointense (usually lesion periphery)	Moderate enhancement of outer margin
Fibrous dysplasia	Low or intermediate signal in ossified or fibrous portions	Increased signal in early resorptive phase Heterogeneous signal in active phase	Maximal enhancement in areas that appear T2 hyperintense
Paget disease	Early destructive to early intermediate phase; Decreased marrow intensity Late sclerotic phase: Marrow hypointense	Marrow changes with marrow replacement	Increased enhancement due to increased vascularity Sarcomatous transformation: mass enhancement, often with central necrosis GCT transformation: enhancing solid tumor areas
Ameloblastoma	Solid tumor parts: low-to-intermediate T1 signal intensity Cystic parts: low-to-intermediate T1 signal intensity	High T2 signal intensity	Solid tumor show strong enhancement seen than in odontogenic cysts Enhancement of mural nodules seen in unicystic variant Cystic areas show no enhancement
Central giant cell granuloma	Hypo to isointense	Hypo to isointense	Heterogeneous enhancement

radiation as suggested by Taner et al., and the masseter was the muscle with highest rate of volume loss and lateral pterygoid showed the highest rate of hyperintensity [53].

Fracture

Magnetic resonance imaging is not usually used for the assessment of facial fracture, but smaller fractures or stress fractures considered having nearly 100% sensitivity. Early MRI features include periosteal and marrow edema, best demonstrated on fluid-sensitive sequences. As the severity of the injury progress, a hypointense linear fracture line may be seen. Periosteal and endosteal new bone formation are hypointense on all sequences [54].

Implantology

Magnetic resonance imaging has been used in the field of dental implantology recently when soft-tissue imaging is required such as location of inferior dental canal and its geometric accuracy is comparable to CT. Main limitations are artifact and heating of the implant which may interfere with osseointegration caused by ferromagnetic type of implant on postimplant evaluation [55]. Dental implant planning, CAD/CAM of a drill guide, and fully guided implant placement were successfully performed in MRI by Flügge, T et al. [56].

Dental MRI

In the conventional MRI, calcified structures of tooth appear as void signal due to highly restricted molecular motion within the mineralised tissues, the signal decay rapidly. SWIFT (Sweep imaging with Fourier transformation), ultrashort echo time (UTE), and zero echo time (ZTE) are all examples of relatively newly developed short T2 pulse sequences with efficacy in imaging hard tissue. SWIFT sequence uses intraoral coil, enabled simultaneous imaging of both soft and hard dental tissues with a high resolution and in a relatively short scanning time (10 min) [57]. The sequence also showed assurance in determining the extent of carious lesions and the status of pulpal tissue, whether reversible or irreversible pulpitis. Bracher et al. [58] reported that the ability of 3D UTE to identify caries lesion is promising.

Dental restorative material and MRI

Awareness among dentists about MR imaging and their interactions with restorative dental materials was limited as per Mathew et al. [59]. Patients with dental restorations may require MRI of the head and neck, which may cause distortion of the images or the dislodgement of the prosthesis which thereby can cause injury to the adjacent tissues, and potentially life-threatening situations could result with certain objects. Careful screening of patients before MRI examinations should be conducted to detect the presence of such materials and to identify their metallic content. Thus, potentially harmful situations can be prevented. Any substances when placed in a magnetic field get magnetized to a degree that depends on their magnetic susceptibility as ferromagnetic, paramagnetic, and diamagnetic [60]. Ferromagnetic materials has high potential to cause the unwanted effect, paramagnetic materials far less likely to cause an artifact and diamagnetic materials are least likely to cause an effect. Variations in the magnetic field strength that occur at the interface between dental materials and the adjacent tissue can lead to spatial distortions and signal loss, thereby generating an artifact in the image. Apart from artifact formation, other unwanted effects of MRI are radiofrequency heating (a physical effect) and magnetically induced displacement (a mechanical effect) of the dental material [61]. Schenck et al. divided the dental restorative material into three groups according to the susceptibility difference; as Compatible, the material produces no detectable distortions, Compatible I, the material produces noticeable distortions, acceptance depends on the application and non-compatible, the material produces strong image distortions even when it is located far from the imaging region [62]. Classification of dental materials based on magnetic susceptibility and its interaction is shown in Table 5.

Contraindications

Due to safety issues, caused by magnetic fields in an MRI scanner, all patients need to be thoroughly screened by healthcare professionals before the scan. The patient's condition, the type of device that patients have, and its compatibility to machine should be evaluated. Contraindications and patients to be more considered while taking MRI scan are mentioned in Table 6. Recently, most medical devices were manufactured as MR safe or MR conditional. Claustrophobic patients who refuse to take MRI scan may need sedation or open MRI systems. MRI is safe during any trimester of pregnancy, to evaluate obstetric and nonobstetric disorders. FDA determines gadolinium as a class C agent, and no known adverse effect reported. Only 0.04% of the gadolinium contrast excreted into breast milk ensures that MRI can be done in lactating mother [63].

Conclusion

The use of MRI in dentistry can be popularized over the coming years, by decreasing the costs and providing better availability. An accurate knowledge on the benefits and limitations of the techniques will further enhance the importance of MRI

Table 5 Classification of materials based on magnetic susceptibility and its interaction

Classification	Type of magnetism	Magnetic susceptibility and its effect	Significance	Dental materials
Compatible	Diamagnetism	Negative susceptibility Internal magnetic field opposes the external field	Fully compatible materials	Composites Glass ionomer cement Guttapercha AH plus resin Acrylic resin Zirconia Pure titanium Gold filling
Compatible I	Paramagnetism	Positive susceptibility Internal magnetic field in the same direction of the external field	Limited distortions	Amalgam Gold alloy Gold ceramic crown Titanium alloy Zinc phosphate cement Metal ceramic Ceramic brackets Nickel titanium wires
Non-compatible	Ferromagnetism	Positive susceptibility Strongly attracted by magnetic field	Strongest distortions	Cobalt chromium alloy Nickel chromium alloy Stainless steel crowns and brackets Ligature and stainless steel wires Metallic endodontic post Metallic dentures

Table 6 Contraindications and patients to be considered while taking MRI scan

Absolute contraindications	Relative contraindications	Patients need to be evaluated before the administration of gadolinium
Cardiac device such as pacemakers, implantable cardioverter	Coronary and peripheral artery stents	Allergic or anaphylactic reaction to gadolinium
Metallic intraocular foreign bodies	Programmable shunts	Dialysis patient
Cochlear/ear implant	Airway stents or tracheostomy	Renal patient with history of renal transplant, single kidney, renal cancer
Implantable neurostimulation systems	Intrauterine device (IUD)	Patients with risk factors for nephrogenic systemic fibrosis
Drug infusion pumps	Ocular prosthesis	Patients under medications for diabetes mellitus or hypertension
Catheters with metallic components	Stapes implants	Patients with glomerular filtration rate below 30 mL/min/1.73 m^2
Hearing aid	Surgical clips or wire sutures	Patients who are pregnant: predicated on a risk–benefit assessment
Metallic fragments such as bullets, shotgun pellets, and metal shrapnel	Penile prosthesis	
Tissue expander	Joint replacement or prosthesis	
Cerebral artery aneurysm clips	Inferior vena cava (IVC) filter:	
Magnetic dental implants	Medication patch	
Artificial limb	Tattoos	
Piercing		

in routine diagnosis, by decreasing the number of invasive diagnostic procedures.

Declarations

Conflict of interest None.

References

1. Purcell EM, Torrey HC, Pound RV. Resonance absorption by nuclear magnetic moments in a solid. Phys Rev. 1946;69:37–8.
2. Grover VP, Tognarelli JM, Crossey MM, Cox IJ, Taylor-Robinson SD, McPhail MJ. Magnetic Resonance Imaging: Principles

and Techniques: Lessons for Clinicians. J ClinExpHepatol. 2015;5(3):246–55.
3. Nooij RP, Hof JJ, van Laar PJ, van der Hoorn A. Functional MRI for treatment evaluation in patients with head and neck squamous cell carcinoma: a review of the literature from a radiologist perspective. Curr Radiol Rep. 2018;6(1):2.
4. Bammer R. Basic principles of diffusion-weighted imaging. Eur J Radiol. 2003;45:169–84.
5. Keevil SF, Barbiroli B, Brooks JC. Absolute metabolite quantification by in vivo NMR spectroscopy: II. A multicentre trial of protocols for in vivo localised proton studies of human brain. Magn Reson Imaging. 1998;16(9):1093–106.
6. Shah GV. MR imaging of salivary glands. Magn Reson Imaging Clin N Am. 2002;10(4):631–62.
7. Yabuuchi H, Fukuya T, Tajima T, Hachitanda Y, Tomita K, Koga M. Salivary gland tumors: diagnostic value of gadolinium-enhanced dynamic MR imaging with histopathologic correlation. Radiology. 2003;226(2):345–54.
8. Yabuuchi H, Matsuo Y, Kamitani T, Setoguchi T, Okafuji T, Soeda H, *et al*. Parotid gland tumors: can addition of diffusion-weighted MR imaging to dynamic contrastenhanced imaging improve diagnostic accuracy in characterization. Radiology. 2008;249(3):909–16.
9. Khamis MEMAA, Ismail EI, Bayomy MF, El-Anwarc MW. The diagnostic efficacy of apparent diffusion coefficient value and Choline/Creatine ratio in differentiation between parotid gland tumors. Egypt J Radiol Nucl Med. 2018;49:358–67.
10. Zhang Y, Ou D, Gu Y, He X, Peng W. Evaluation of salivary gland function using diffusion-weighted magnetic resonance imaging for follow-up of radiation-induced xerostomia. Korean J Radiol. 2018;19(4):758–66.
11. Regier M, Ries T, Arndt C, *et al*. Sjögren's syndrome of the parotid gland: value of diffusion-weighted echo-planar MRI for diagnosis at an early stage based on MR sialography grading in comparison with healthy volunteers. Rofo. 2009;181(3):242–8.
12. Terra GTC, Oliveira JXD, Hernandez A, Lourenço SV, Arita ES, Cortes ARG. Diffusion-weighted MRI for differentiation between sialadenitis and pleomorphic adenoma. Dentomaxillofac Radiol. 2017;46:20160257.
13. Sumi M, CauterenSumiObaraIchikawaNakamura MVTMYT. Salivary gland tumors: use of intravoxel incoherent motion MR imaging for assessment of diffusion and perfusion for the differentiation of benign from malignant tumors. Radiology. 2012;263(3):770–7.
14. Roberts C, Parker GJ, Rose CJ, *et al*. Glandular function in Sjögren syndrome: assessment with dynamic contrast-enhanced MR imaging and tracer kinetic modeling–initial experience. Radiology. 2008;246(3):845–53.
15. King AD, David KW, Ahuja AT, Gary MK, Yuen HY, Wong KT, Andrew C. Salivary gland tumors at in vivo proton MR spectroscopy. Radiology. 2005;237(2):563–9.
16. Ahmed NS, Mansour SM, El-Wakd MM, Al-Azizi HM, Abu-Taleb NS. The value of magnetic resonance sialography and magnetic resonance imaging versus conventional sialography of the parotid gland in the diagnosis and staging of Sjögren's syndrome. Egypt Rheumatol. 2011;33(3):147–54.
17. Kalinowski M, Heverhagen JT, Rehberg E, Klose KJ, Wagner HJ. Comparative study of MR sialography and digital subtraction sialography for benign salivary gland disorders. AJNR Am J Neuroradiol. 2002;23(9):1485–92.
18. Trotta BM, Pease CS, John Rasamny Jk, Raghavan P, Mukherje S. Oral cavity and oropharyngeal squamous cell cancer: key imaging findings for staging and treatment planning. Radiographics. 2011;31(2):339–54.
19. Chawla S, Kim S, Wang S, Poptani H. Diffusion-weighted imaging in head and neck cancers. Future Oncol. 2009;5(7):959–75.
20. Kitamoto E, Chikui T, Kawano S, Ohga M, Kobayashi K, Matsuo Y, Yoshiura T, Obara M, Honda H, Yoshiura K. The application of dynamic contrast-enhanced MRI and diffusion-weighted MRI in patients with maxillofacial tumors. Acad Radiol. 2015;22(2):210–6.
21. Abdel Razek AA, Poptani H. MR spectroscopy of head and neck cancer. Eur J Radiol. 2013;82(6):982–9.
22. Wang J, Takashima S, Takayama F, Kawakami S, Saito A, Matsushita T, Momose M, Ishiyama T. Head and neck lesions: characterization with diffusion-weighted echo-planar MR imaging. Radiology. 2001;220:621–30.
23. Razek AA. Diffusion tensor imaging in differentiation of residual head and neck squamous cell carcinoma from post-radiation changes. Magn Reson Imaging. 2018;1(54):84–9.
24. Vandecaveye V, De Keyzer F, Vander Poorten V, Dirix P, Verbeken E, Nuyts S, *et al*. Head and neck squamous cell carcinoma: value of diffusion-weighted MR imaging for nodal staging. Radiology. 2009;251(1):134–46.
25. Kim S, Loevner L, Quon H, *et al*. Diffusion-weighted magnetic resonance imaging for predicting and detecting early response to chemoradiation therapy of squamous cell carcinomas of the head and neck. Clin Cancer Res. 2009;15:986–94.
26. Park M, Kim J, Choi YS, Seung-Koo L, Woo Koh Y, Se-Heon Kim K, Chang Choi E. Application of dynamic contrast-enhanced MRI parameters for differentiating squamous cell carcinoma and malignant lymphoma of the oropharynx. Am J Roentgenol. 2016;206(2):401–7.
27. Shukla-Dave A, Lee NY, Jansen JF, *et al*. Dynamic contrast-enhanced magnetic resonance imaging as a predictor of outcome in head-and-neck squamous cell carcinoma patients with nodal metastases. Int J Radiat Oncol Biol Phys. 2012;82(5):1837–44.
28. Fujima N, Kudo K, Yoshida D, *et al*. Arterial spin labeling to determine tumor viability in head and neck cancer before and after treatment. J Magn Reson Imaging. 2014;40:920–8.
29. Mukherji SK, Schiro S, Castillo M, Kwock L, Muller KE, Blackstock W. Proton MR spectroscopy of squamous cell carcinoma of the extracranial head and neck: in vitro and in vivo studies. Am J Neuroradiol. 1997;18:1057–72.
30. Yu Q, Yang J, Wang P, Shi H, Luo J. Preliminary assessment of benign maxillofacial and neck lesions with in vivo single-voxel 1H magnetic resonance spectroscopy. Oral Surg Oral Med Oral Pathol Oral Radiol Endod. 2007;104:264–70.
31. Bezabeh T, Odlum O, Nason R, *et al*. Prediction of treatment response in head and neck cancer by magnetic resonance spectroscopy. Am J Neuroradiol. 2005;26:2108–13.
32. King A, Yeung D, Yu K, *et al*. Monitoring of treatment response after chemoradiotherapy for head and neck cancer using in vivo 1H MR spectroscopy. Eur Radiol. 2010;20:165–72.
33. Sanjay SK, Mukesh HG. Magnetic resonance techniques in lymph node imaging. Appl Radiol. 2004;33(7):34–44.
34. Forghani R, Yu E, Levental M, Som PM, Curtin HD. Imaging evaluation of lymphadenopathy and patterns of lymph node spread in head and neck cancer. Expert Rev Anticancer Ther. 2015;15(2):207–24.
35. Tomas X, Pomes J, Berenguer J, *et al*. MR imaging of temporomandibular joint dysfunction: a pictorial review. Radiographics. 2006;26(3):765–81.
36. Ashraf Baba I, Najmuddin M, Farooq Shah A, Yousuf A. TMJ imaging: a review. Int J Contemp Med Res. 2016;3(8):2253–6.
37. Ahmad M, Hollender L, Anderson Q, *et al*. Research diagnostic criteria for temporomandibular disorders (RDC/TMD): development of image analysis criteria and examiner reliability for image analysis. Oral Surg Oral Med Oral Pathol Oral Radiol Endod. 2009;107(6):844–60.
38. Venetis G, Pilavaki M, Triantafyllidou K, Papachristodoulou A, Lazaridis N, Palladas P. The value of magnetic

resonance arthrography of the temporomandibular joint in imaging disc adhesions and perforations. Dentomaxillofac Radiol. 2011;40(2):84–90.
39. Zhang J, Gersdorff S, Frahm N. Real-time magnetic resonance imaging of temporomandibular joint dynamics. Open Med Imaging J. 2011;511:1–7.
40. Bhat V, Salins PC, Bhat V. Imaging spectrum of hemangioma and vascular malformations of the head and neck in children and adolescents. J Clin Imaging Sci. 2014;24(4):31.
41. Dong MJ, Zhou GY, Sun Q, Wang PZ, Yu Q, Qiang SK, Xue Yi. Evaluation of MR diffusion-weighted imaging (MR-DWI) between head and neck hemangioma and venous. J Stomatol. 2010;19(4):378–82.
42. Chhabra A, Bajaj G, Wadhwa V, Quadri RS, White J, Myers LL, Amirlak B, Zuniga JR. MR neurographic evaluation of facial and neck pain: normal and abnormal craniospinal nerves below the skull base. Radiographics. 2018;38(5):1498–513.
43. Skolnik AD, Loevner LA, Sampathu DM, Newman JG, Lee JY, Bagley LJ, Kim O. Cranial nerve Schwannomas: diagnostic imaging approach learned. Radiographics. 2016;36(5):1463–77.
44. Kurabayashi T, Ida M, Yasumoto M, *et al*. MRI of ranulas. Neuroradiology. 2000;42(12):917–22.
45. Boeddinghaus R, Whyte A. Current concepts in maxillofacial imaging. Eur J Radiol. 2008;66:396–418.
46. García-Ferrer L, Bagán JV, Martínez-Sanjuan V, Hernandez-Bazan S, García R, Jiménez-Soriano Y, Hervas V. MRI of mandibular osteonecrosis secondary to bisphosphonates. Am J Roentgenol. 2008;190(4):949–55.
47. Avril L, Lombardi T, Ailianou A, *et al*. Radiolucent lesions of the mandible: a pattern-based approach to diagnosis. Insights Imaging. 2014;5(1):85–101.
48. Kapoor S. Comparative evaluation of ultrasonography and MRI in detection of odontogenic fascial space infections: a prospective study. Int J Med Res Health Sci. 2019;8(5):45–51.
49. Hayeri MR, PouyaZiai ML, Shehata OM, Teytelboym OM, Huang BK. Soft-tissue infections and their imaging mimics: from cellulitis to necrotizing fasciitis. RadioGraphics. 2016;36(6):188–91.
50. Zhang S, Olthoff A, Frahm J. Real-time magnetic resonance imaging of normal swallowing. J Magn Reson Imaging. 2012;35(6):1372–9.
51. Ekprachayakoon I, Miyamoto JJ, Inoue-Arai MS, Honda EI, Takada JI, Kurabayashi T, Moriyama K. New application of dynamic magnetic resonance imaging for the assessment of deglutitive tongue movement. Prog Orthod. 2018;19(1):45.
52. Sawada E, *et al*. Increased apparent diffusion coefficient values of masticatory muscles on diffusion-weighted magnetic resonance imaging in patients with temporomandibular joint disorder and unilateral pain. J Oral Maxillofacial Surg. 2019;77(11):2223–9.
53. A Taner et.al (2019). Radiotherapy induced changes of masticatory muscles and parotid glands on MRI in patients with nasopharyngeal carcinoma
54. Marshall RA, Mandell JC, Weaver MJ, Ferrone M, Sodickson A, Khurana B. Imaging features and management of stress, a typical, and pathologic fractures. Radiographics. 2018;38(7):2173–92.
55. Hussain MW, Chaudhary MAG, Ahmed AR, *et al*. Latest trends in imaging techniques for dental implant: a literature review. Int J Radiol Radiat Ther. 2017;3(5):288–90.
56. Flügge T, Ludwig U, Hövener J-B, Kohal R, Wismeijer D, Nelson K. Virtual implant planning and fully guided implant surgery using magnetic resonance imaging—proof of principle. Clin Oral Impl Res. 2020;00:1–9.
57. DemirturkKocasarac H, Geha H, Gaalaas LR, Nixdorf DR. MRI for dental applications. Dent Clin North Am. 2018;62(3):467–80.
58. Bracher AK, Hofmann C, Bornstedt A, *et al*. Ultrashort echo time (UTE) MRI for the assessment of caries lesions. Dentomaxillofac Radiol. 2013;42(6):20120321.
59. Mathew CA, Maller SV, Maller US, Maheshwaran M, Valarmathi S, Karrunakaran B. Evaluation of awareness among dentists about magnetic resonance imaging and their interactions with restorative dental materials: a survey among dentists in three districts of Tamilnadu. J Indian Acad Dent Spec Res. 2016;3:6–9.
60. Costa AL, Appenzeller S, Yasuda CL, Pereira FR, Zanardi VA, Cendes F. Artifacts in brain magnetic resonance imaging due to metallic dental objects. Med Oral Patol Oral Cir Bucal. 2009;14:E278–82.
61. Mathew CA, Maheswaran SM. Interactions between magnetic resonance imaging and dental material. J Pharm Bioallied Sci. 2013;5(Suppl 1):113–6.
62. Schenck JF. The role of magnetic susceptibility in magnetic resonance imaging: MRI magnetic compatibility of the first and second kinds. Med Phys. 1996;23:815–50.
63. Ghadimi M, Sapra A (2020) Magnetic resonance imaging (MRI), contraindications. [Updated 2020 May 24]. In: StatPearls [Internet]. Treasure Island (FL): StatPearls Publishing; 2020 Jan. Available from: https://www.ncbi.nlm.nih.gov/books/NBK551669/